Supporting information for

Supramolecular self-assembly of heterobimetallic complexes: A new N,P-based, selective heteroditopic ligand

Daniel John Hutchinson, Reike Clauss, Menyhárt-Botond Sárosi, and Evamarie Hey-Hawkins*

Faculty of Chemistry and Mineralogy, Institute of Inorganic Chemistry, Leipzig University, D-04103 Leipzig, Germany. E-mail: hey@uni-leipzig.de

Table of Contents

1. X-ray crystallographic data

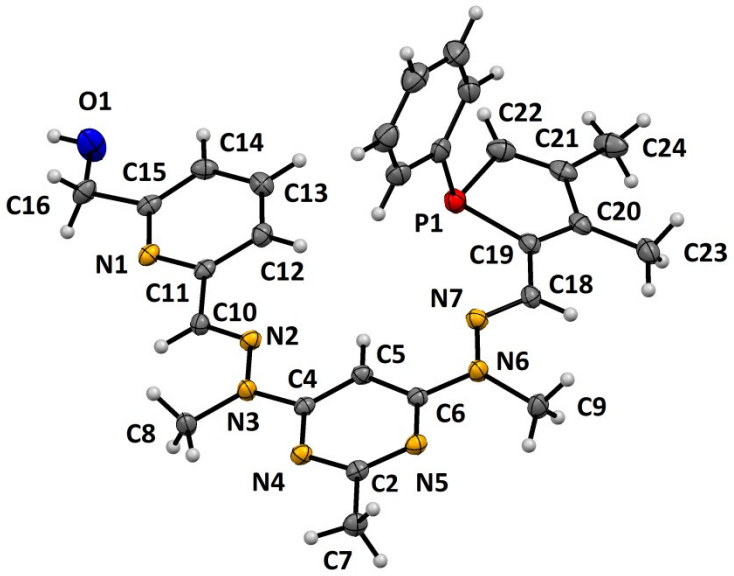

Figure S1. View of the solid-state form of ligand **L1**. Thermal ellipsoids are drawn at the 50% probability level. Selected bond lengths [Å]: O1-C16 1.400(2), P1-C19 1.818(2), P1-C22 1.792(2), P1-C25(Ph) 1.839(2). Selected bond angles [°]: C19-P1-C22 89.47(7), C19-P1-C25(Hh) 102.44(7).

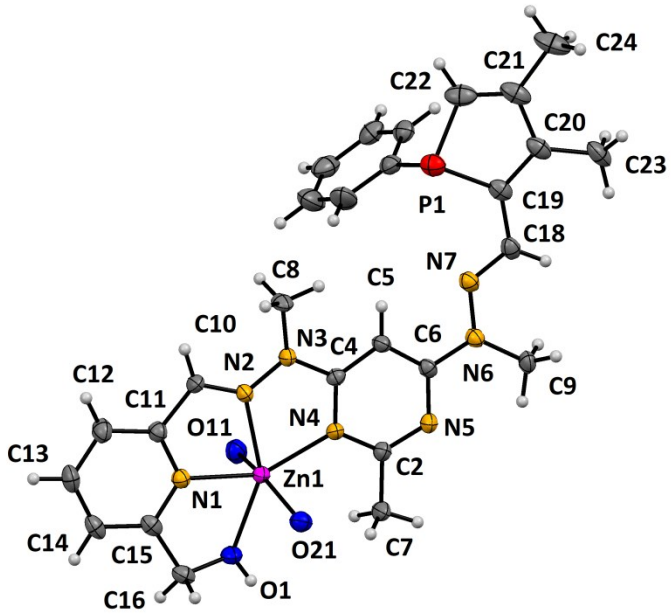

Figure S2. View of the solid-state form of [Zn**L1**$(SO_3CF_3)_2$]. The coordinated $SO_3CF_3^-$ anions, but O11 and O21, have been removed for clarity. Thermal ellipsoids are drawn at the 50% probability level. Selected bond lengths [Å]: Zn1-O1 2.133(2), Zn1-N1 2.070(3), Zn1-N2 2.163(2), Zn1-N4 2.057(4), Zn1-O11 2.112(2), Zn1-O21 2.209(2), P1-C19 1.826(3), P1-C22 1.803(3), P1-C25(Ph) 1.835(4). Selected bond angles [°]: O1-Zn1-N4 136.11(9), O1-Zn1-N1 75.13(9), O1-Zn1-O11 84.18(9), O11-Zn1-O21 160.25(9), C19-P1-C22 88.9(2), C19-P1-C25(Ph) 102.5(1).

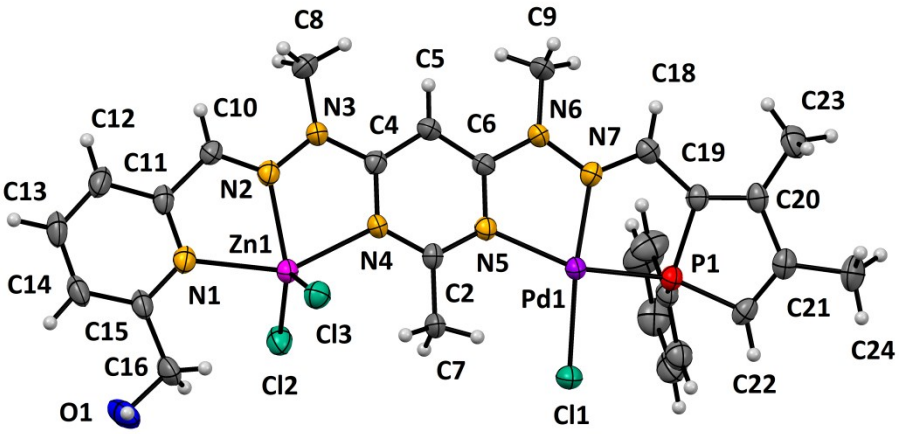

Figure S3. View of the solid-state form of [ZnPd**L1**Cl_3]$(SO_3CF_3)\cdot C_7H_8\cdot CH_3NO_2$. The uncoordinated C_7H_8 molecule was removed for clarity. The uncoordinated $SO_3CF_3^-$ anion and CH_3NO_2 molecule were removed by SQUEEZE due to disorder. Thermal ellipsoids are drawn at the 50% probability level. Selected bond lengths [Å]: Zn1-N1 2.203(3), Zn1-N2 2.122(3), Zn1-N4 2.211(3), Zn1-Cl2 2.275(1), Zn1-Cl3 2.463(1), Pd1-N5 2.140(3), Pd1-N7 2.010(3), Pd1-P1 2.193(1), P1-C19 1.801(4), P1-C22 1.788(4), P1-C25(Ph) 1.807(5). Selected bond angles [°]: N1-Zn1-N2 75.1(1), N2-Zn1-N4 75.5(1), N2-Zn1-Cl3 119.4(1), Cl2-Zn1-Cl3 125.72(5), N5-Pd1-N7 77.7(1), N7-Pd1-P1 84.5(1), P1-Pd1-Cl1 87.43(4), N5-Pd1-P1 161.4(1), N7-Pd1-Cl1 171.1(1), C19-P1-C22 92.9(2), C19-P1-C25(Ph) 110.8(2).

2. DFT results

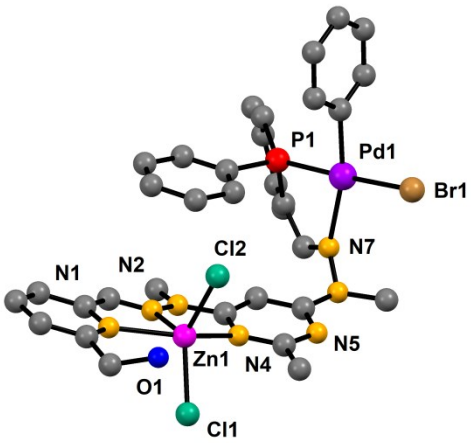

1a: 0.00 kJ mol^{-1}

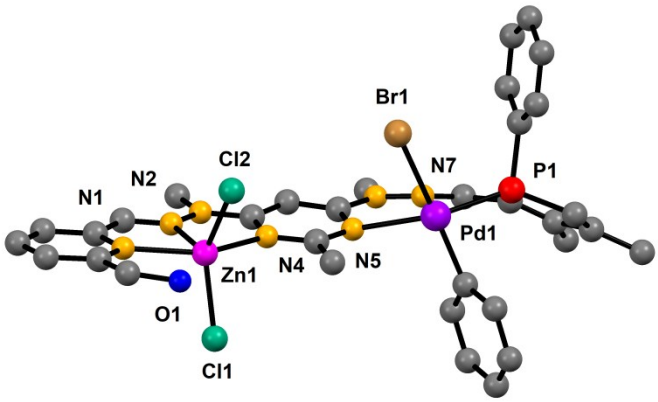

1b: +16.30 kJ mol^{-1}

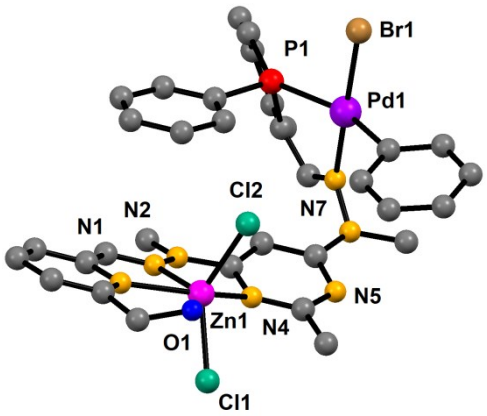

1c: +26.70 kJ mol^{-1}

Figure S4. Optimised geometries of the oxidative addition products of [ZnPd^0**L1**Cl$_2$] and PhBr and the corresponding relative Gibbs free enthalpies. Selected calculated distances and Wiberg bond indices: **1a**, Pd1–P1: 2.259 Å (0.92), Pd1···N5: 4.812 Å (< 0.05), Pd1–N7: 2.318 Å (0.36), Pd1–Br1: 2.559 Å (0.80), Pd1–C(Ph): 2.030 Å (0.94); **1b**, Pd1–P1: 2.258 Å (1.00), Pd1–N5: 2.427 Å (0.25), Pd1···N7: 2.644 Å (0.15), Pd1–Br1: 2.607 Å (0.74), Pd1–C(Ph): 2.030 Å (0.94); **1c**, Pd1–P1: 2.421 Å (0.70), Pd1···N5: 4.662 Å (< 0.05), Pd1–N7: 2.150 Å (0.51), Pd1–Br1: 2.500 Å (0.90), Pd1–C(Ph): 2.038 Å (0.92).

3. ^{1}H, ^{31}P, and ^{13}C NMR data of L1 and its complexes

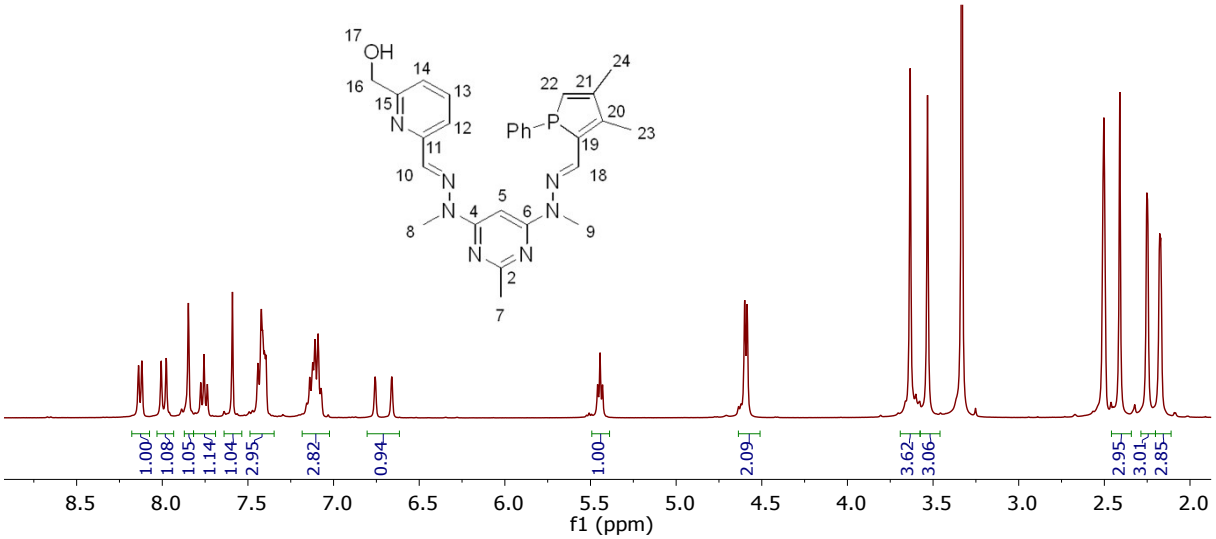

Figure S5. ^{1}H NMR spectrum of **L1**.

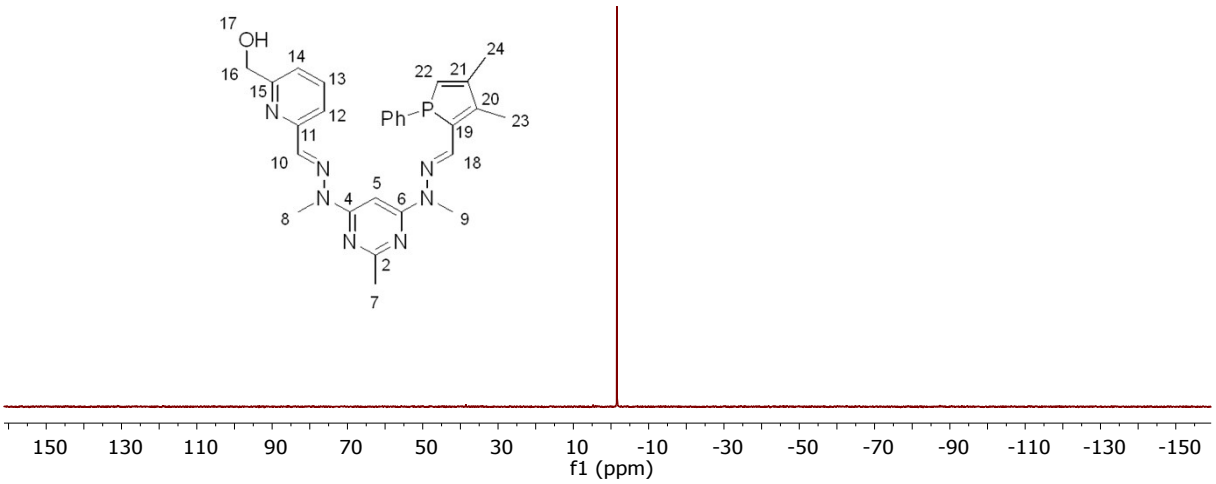

Figure S6. $^{31}P\{^{1}H\}$ NMR spectrum of **L1**.

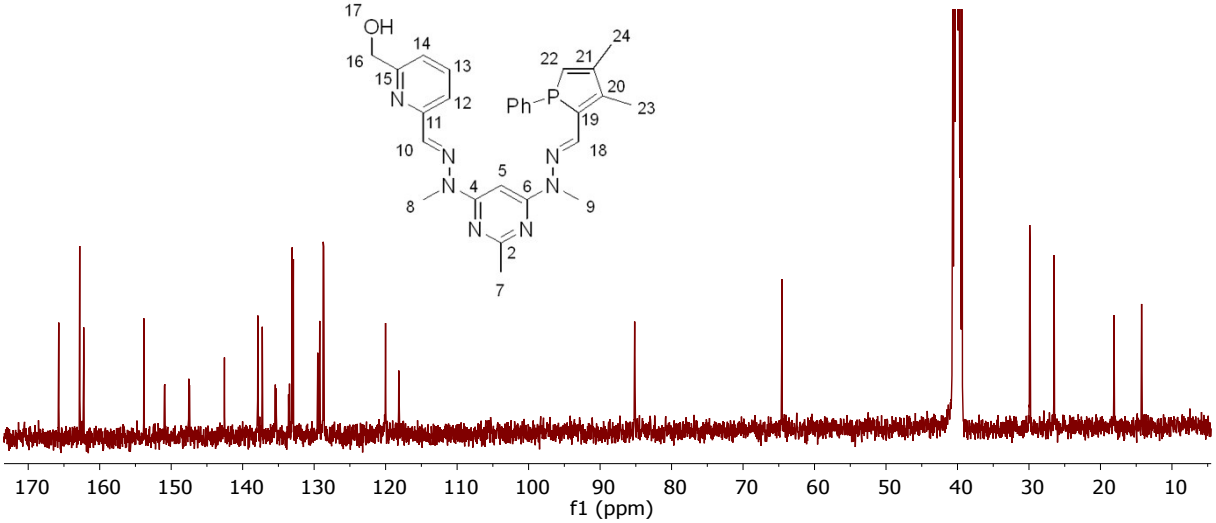

Figure S7. $^{13}C\{^{1}H\}$ NMR spectrum of **L1**.

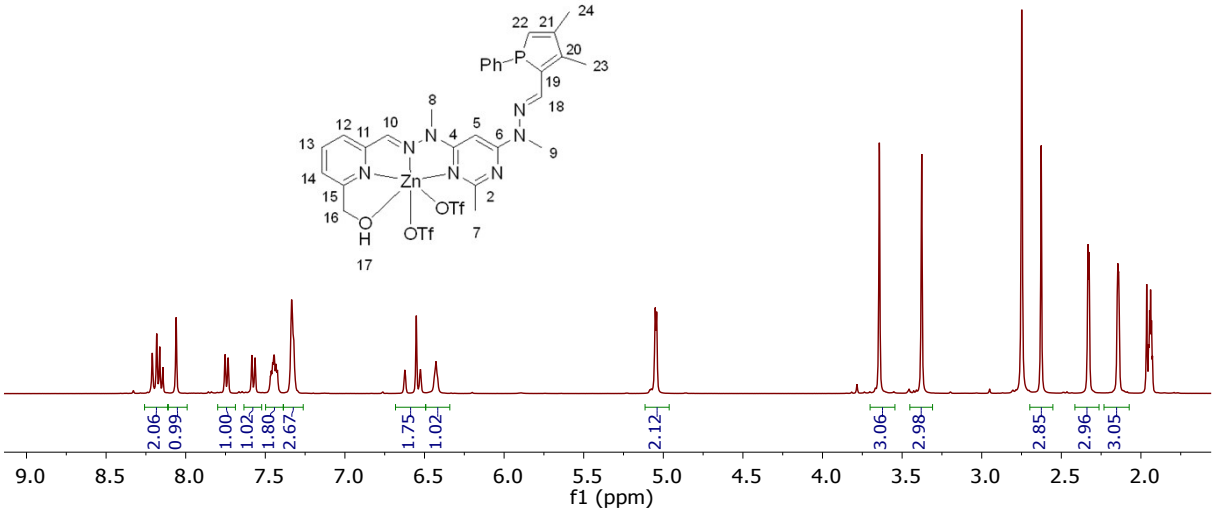

Figure S8. ^{1}H NMR spectrum of [Zn**L1**$(SO_3CF_3)_2$].

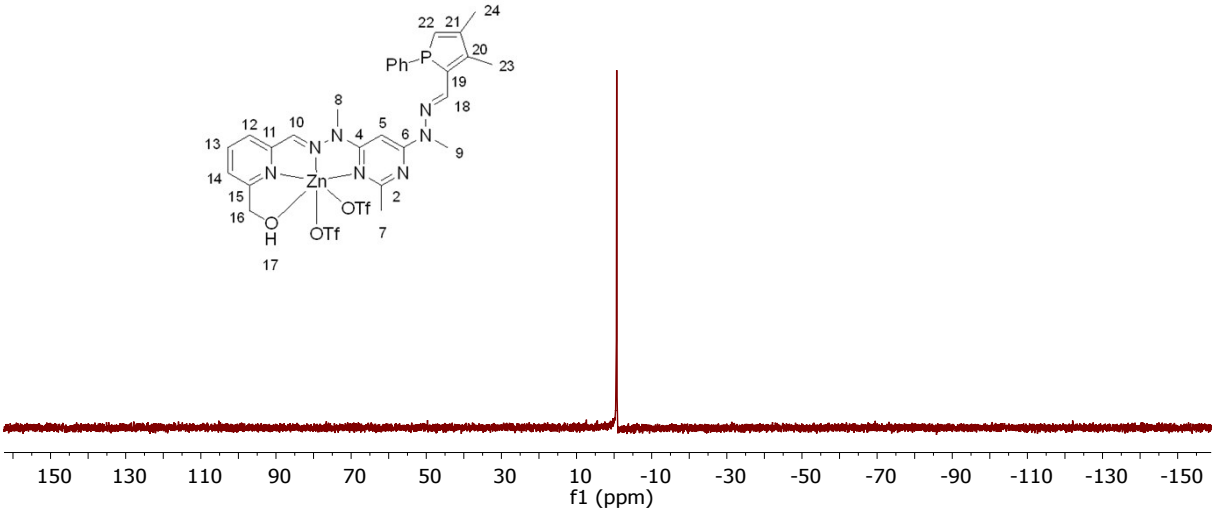

Figure S9. $^{31}P\{^{1}H\}$ NMR spectrum of [Zn**L1**$(SO_3CF_3)_2$].

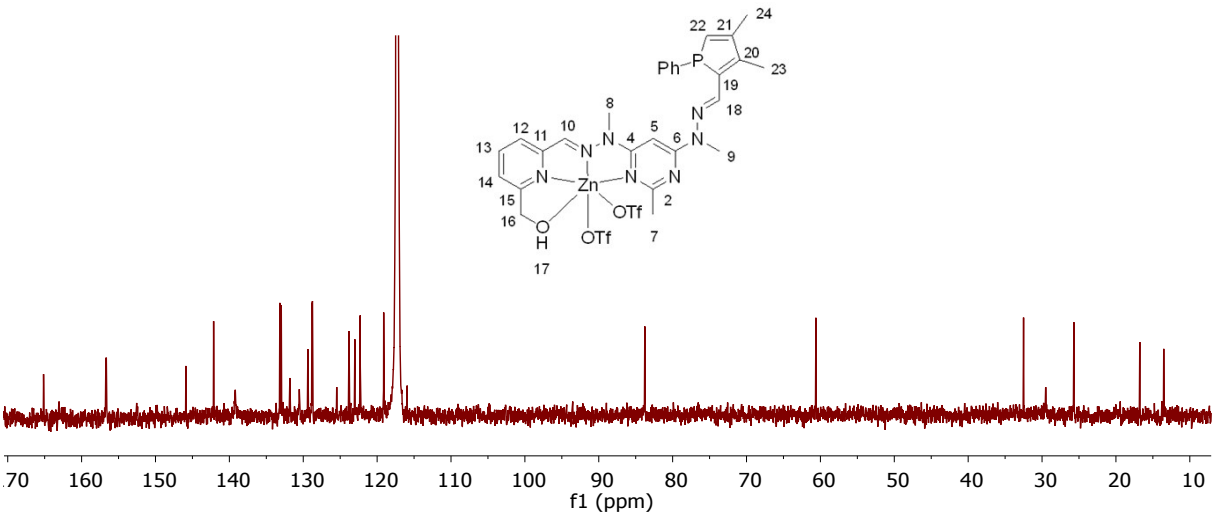

Figure S10. $^{13}C\{^{1}H\}$ NMR spectrum of [Zn**L1**$(SO_3CF_3)_2$].

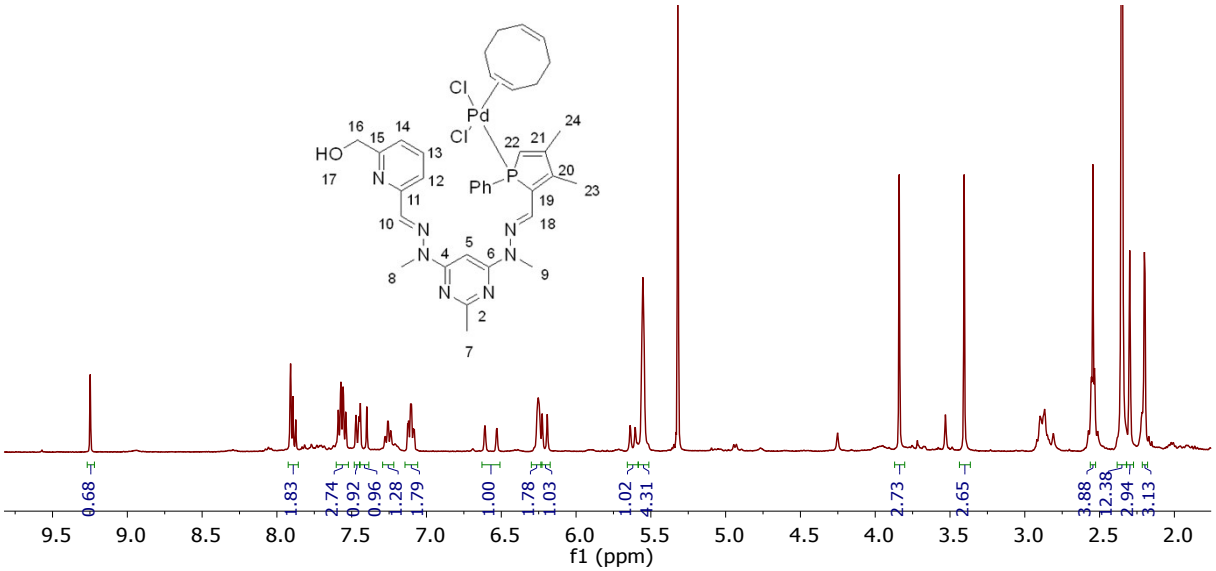

Figure S11. ^{1}H NMR spectrum of [Pd**L1**Cl$_2$(COD)].

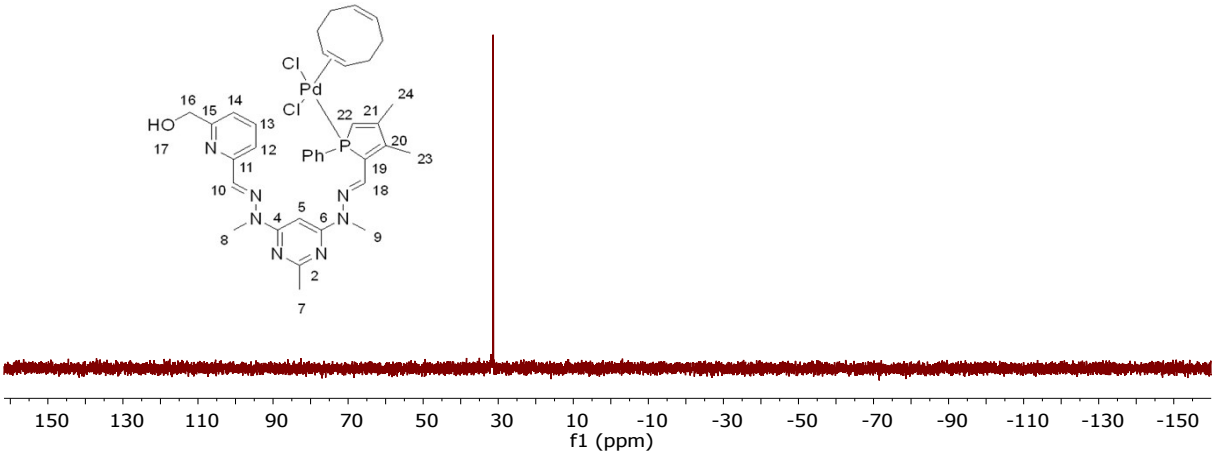

Figure S12. ^{31}P{^{1}H} NMR spectrum of [Pd**L1**Cl$_2$(COD)].

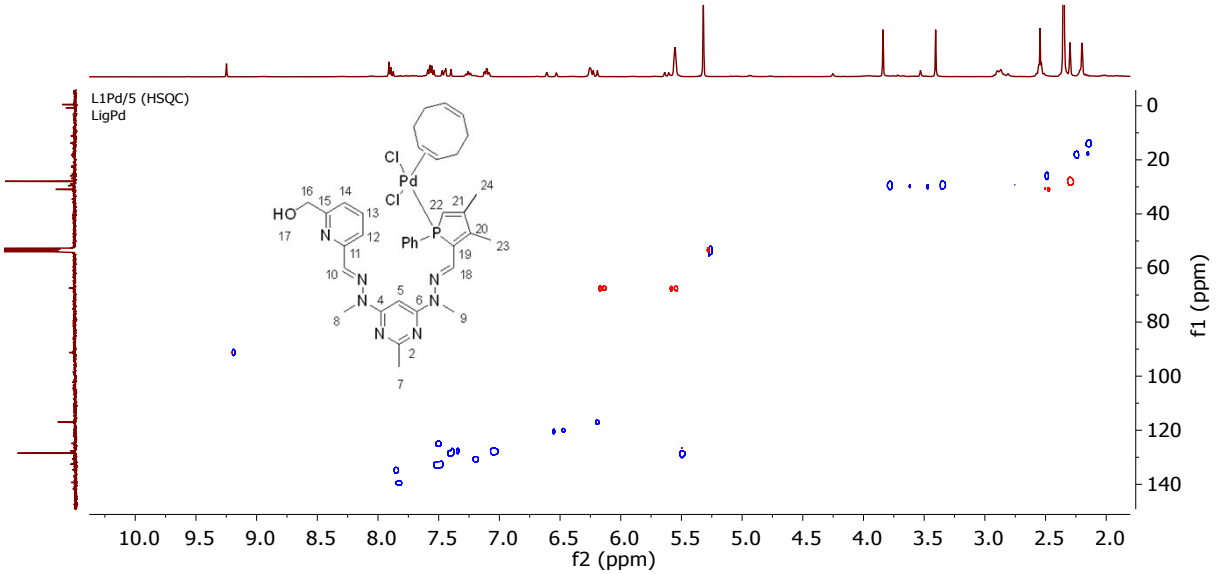

Figure S13. HSQC spectrum of [Pd**L1**Cl$_2$(COD)], used to assign the ^{13}C NMR peaks as the signals in the ^{13}C NMR spectrum itself were too weak.

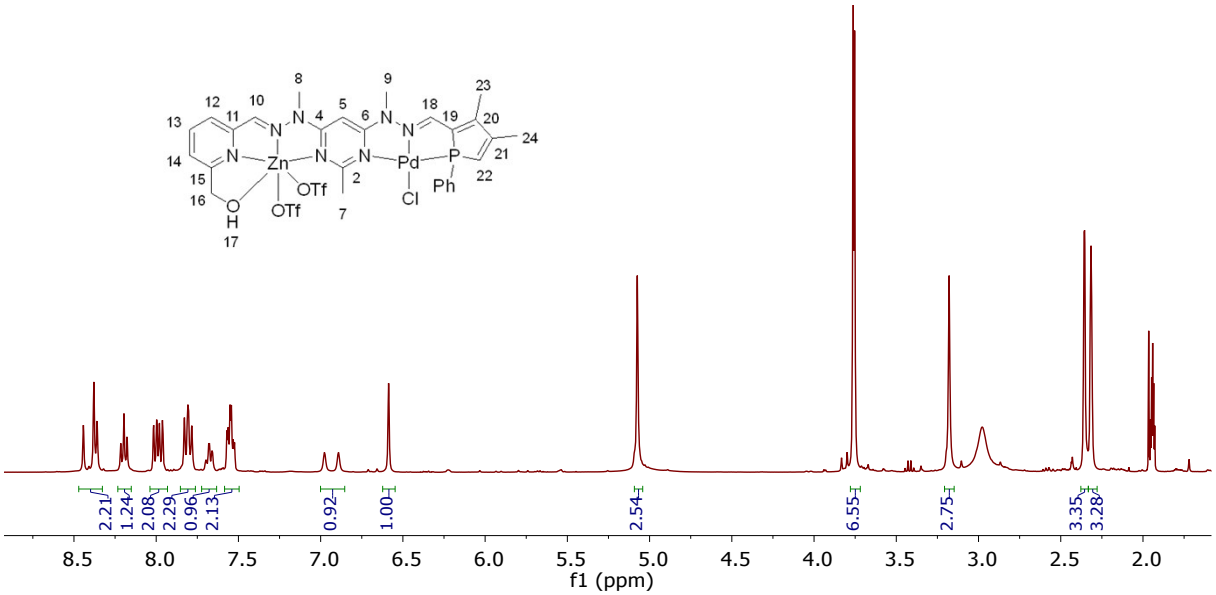

Figure S14. ^{1}H NMR spectrum of [ZnPd**L1**$Cl_2(SO_3CF_3)_2$].

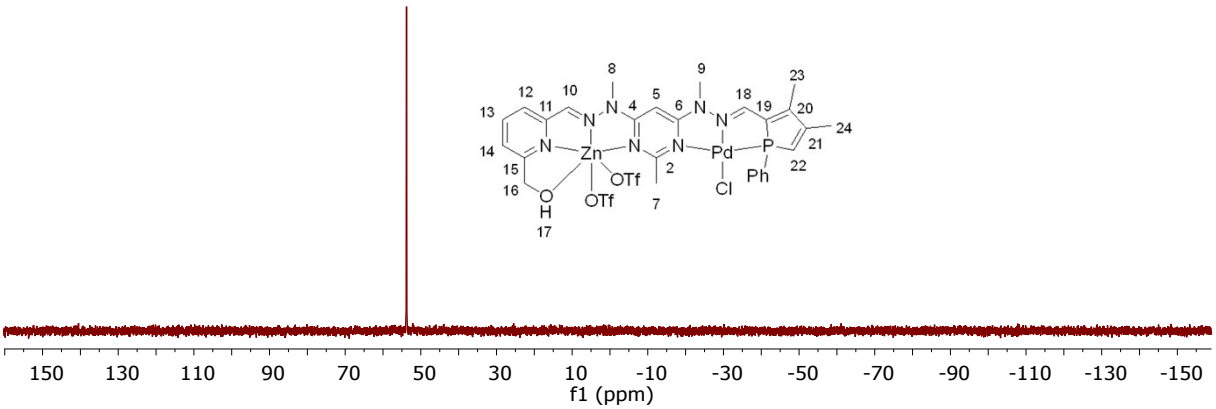

Figure S15. ^{31}P{^{1}H} NMR spectrum of [ZnPd**L1**$Cl_2(SO_3CF_3)_2$].

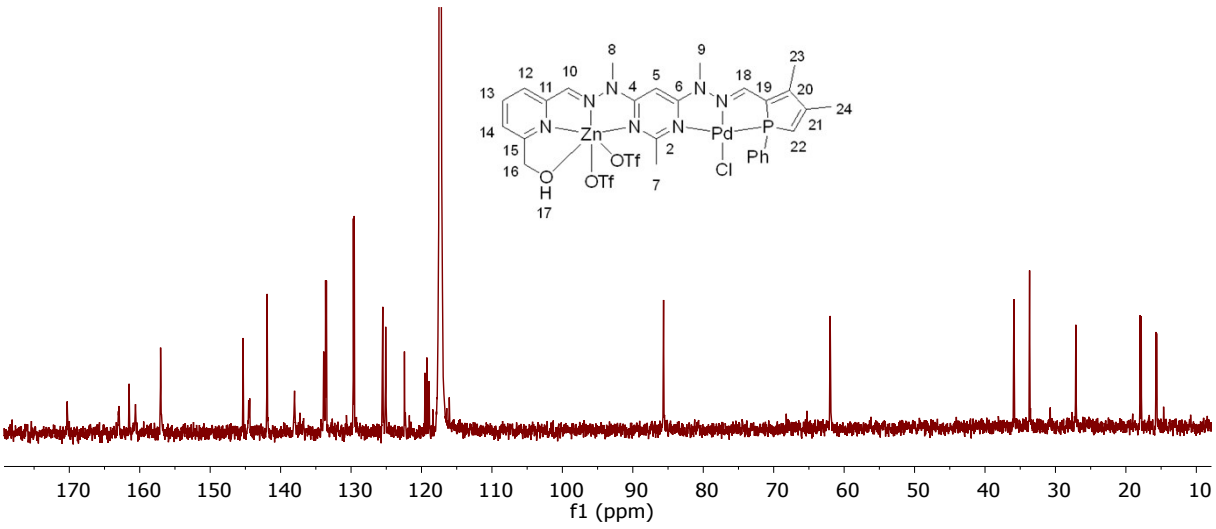

S16. ^{13}C{^{1}H} NMR spectrum of [ZnPd**L1**$Cl_2(SO_3CF_3)_2$].

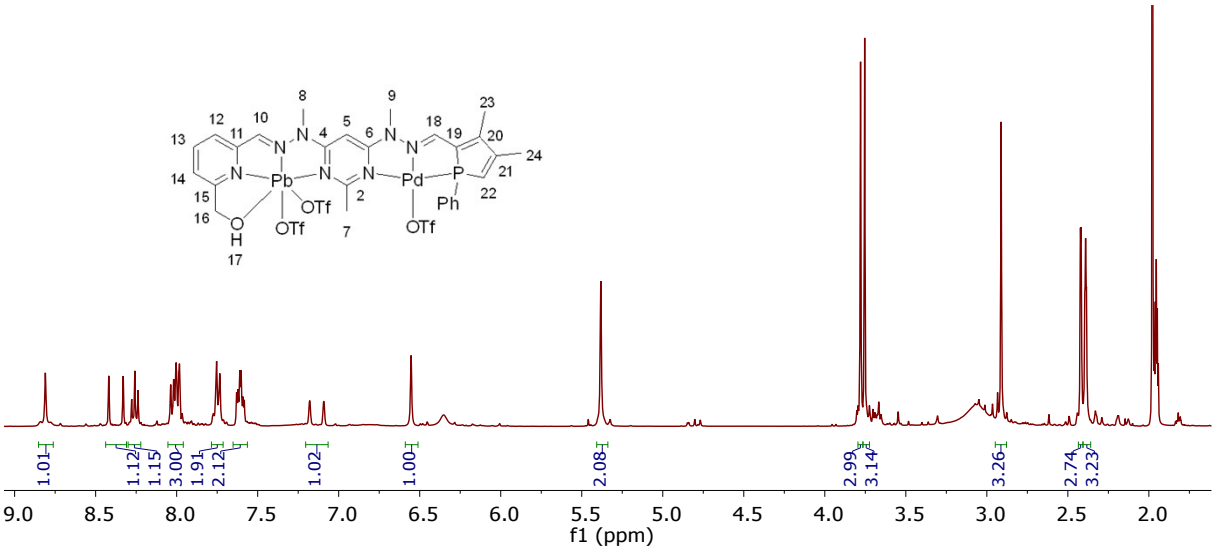

Figure S17. ^{1}H NMR spectrum of [PbPd**L1**$(SO_3CF_3)_4$].

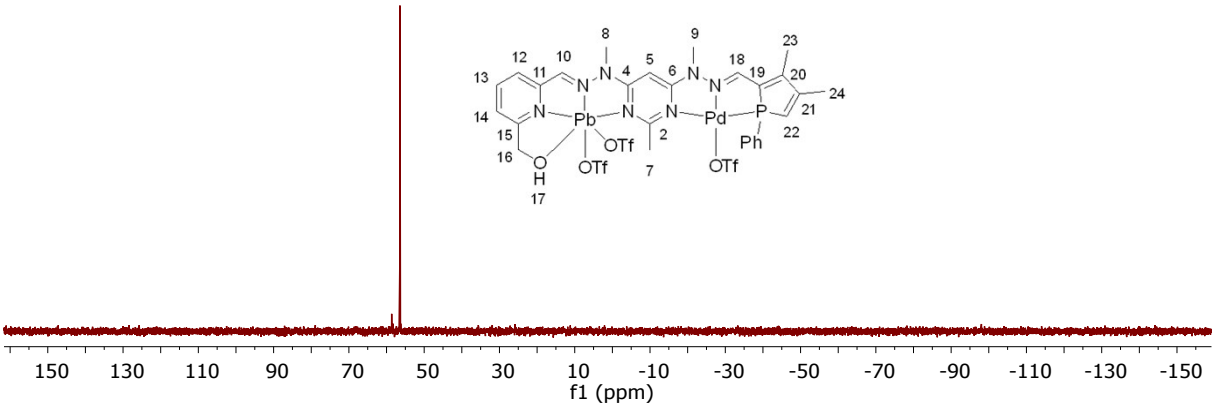

Figure S18. $^{31}P\{^{1}H\}$ NMR spectrum of [PbPd**L1**$(SO_3CF_3)_4$]

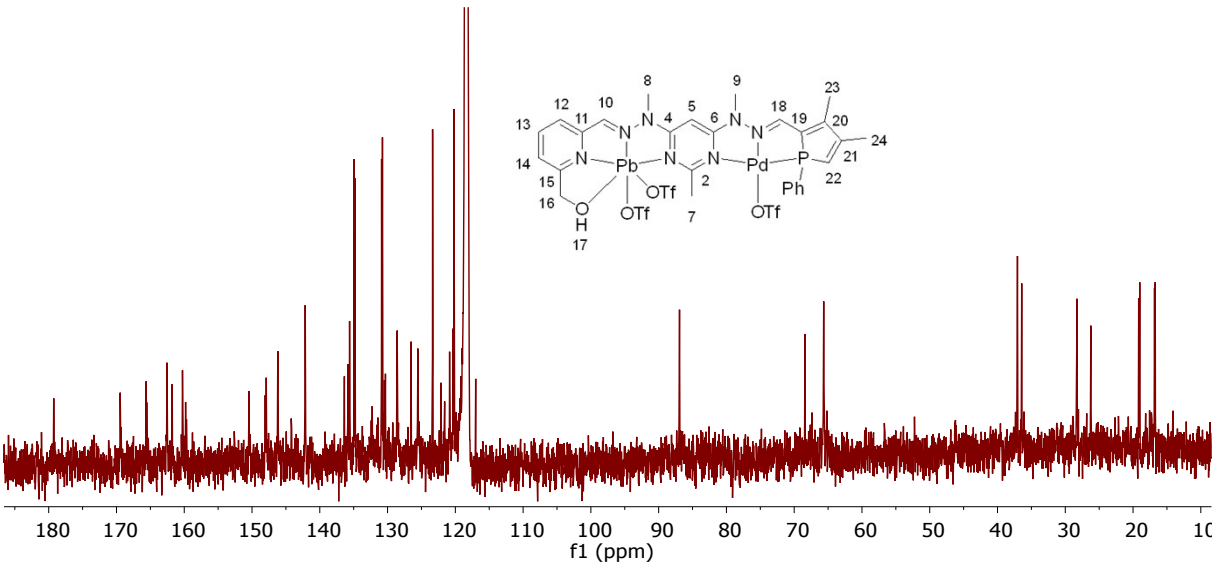

Figure S19. $^{13}C\{^{1}H\}$ NMR spectrum of [PbPd**L1**$(SO_3CF_3)_4$].

4. IR data of L1 and its complexes

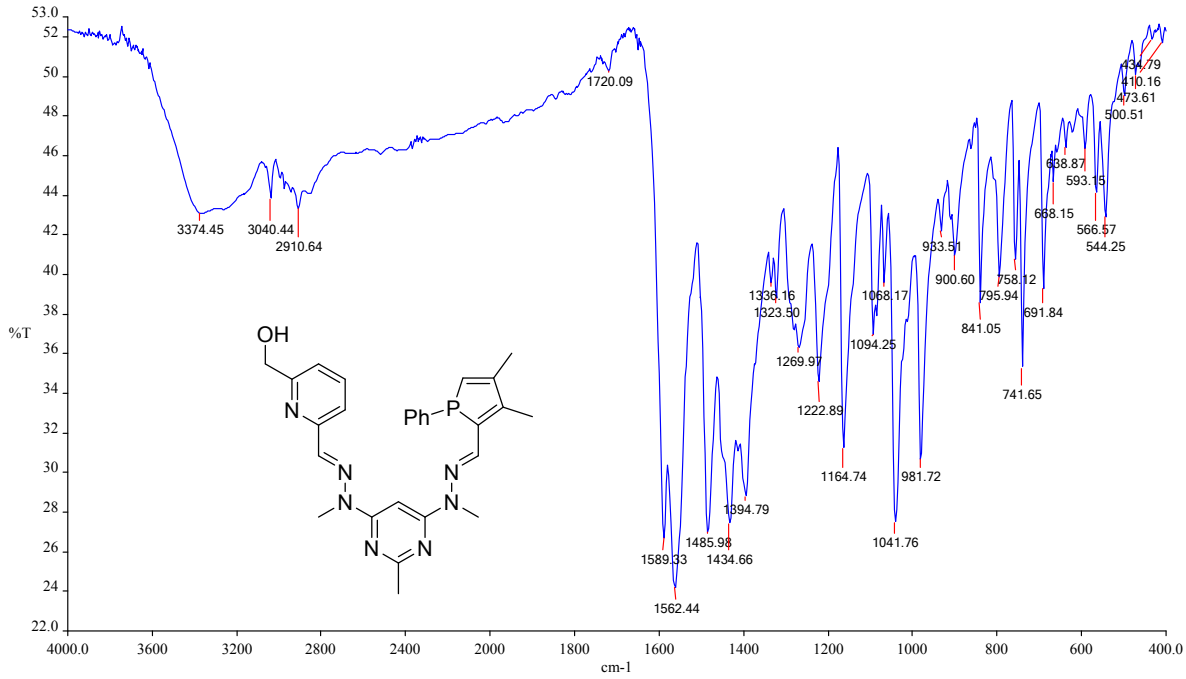

Figure S20. IR (KBr) spectrum of **L1**.

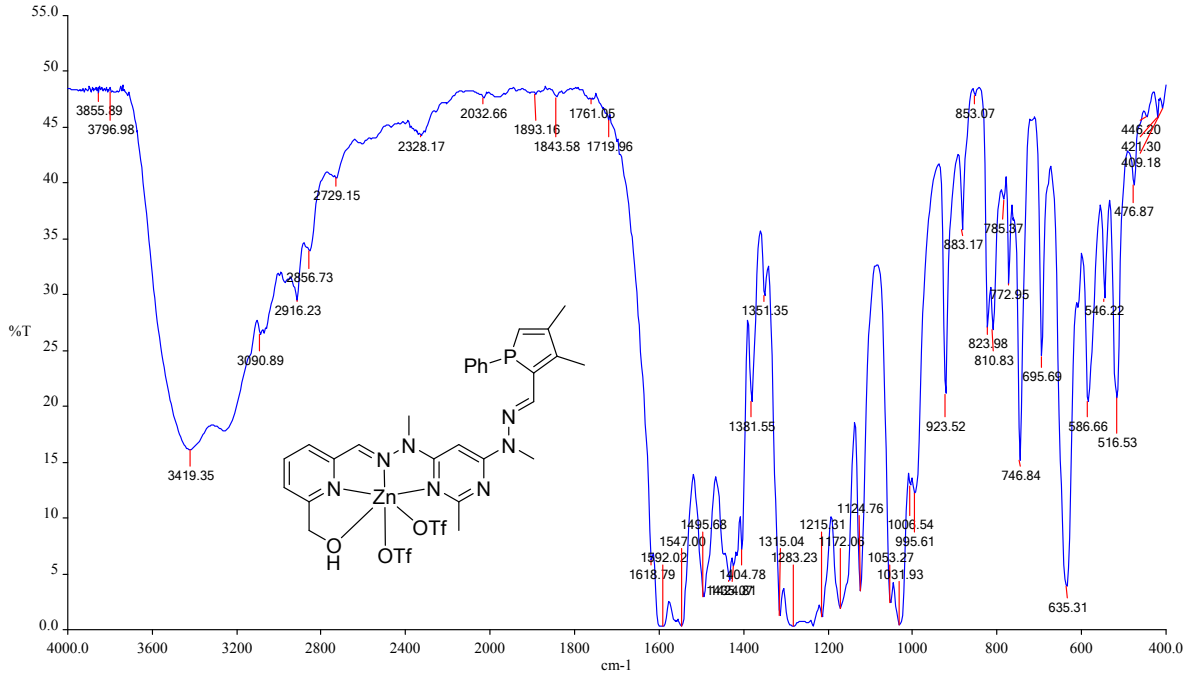

Figure S21. IR (KBr) spectrum of [Zn**L1**$(SO_3CF_3)_2$].

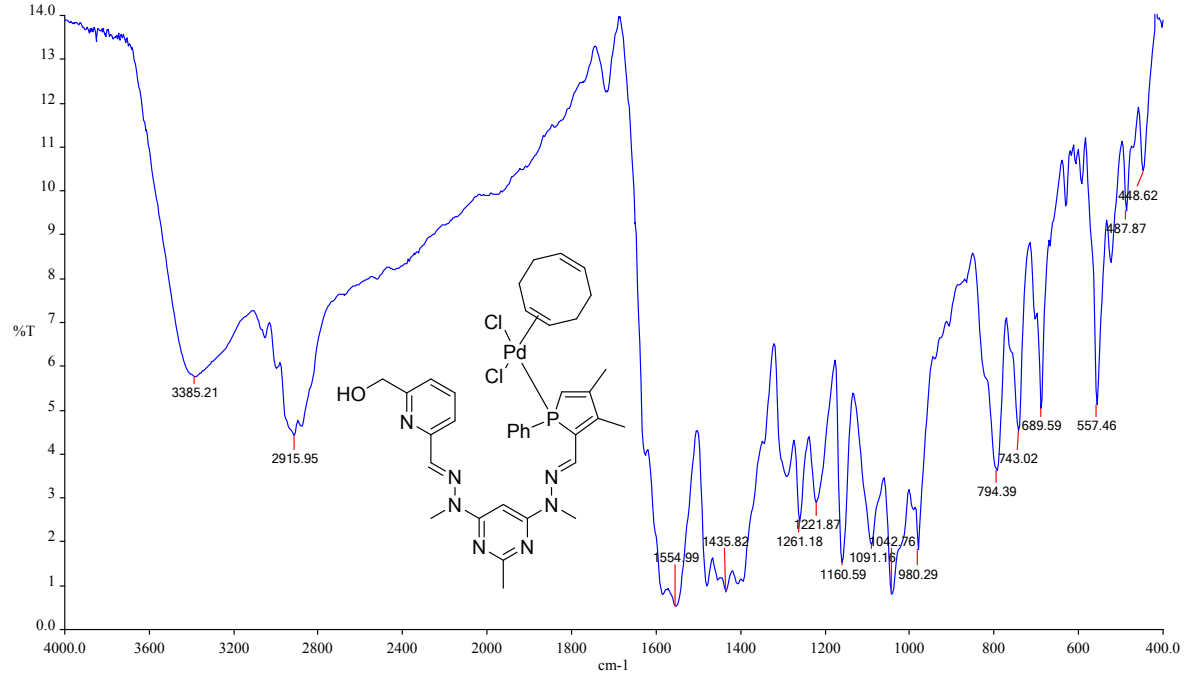

Figure S22. IR (KBr) spectrum of [Pd**L1**Cl_2(COD)].

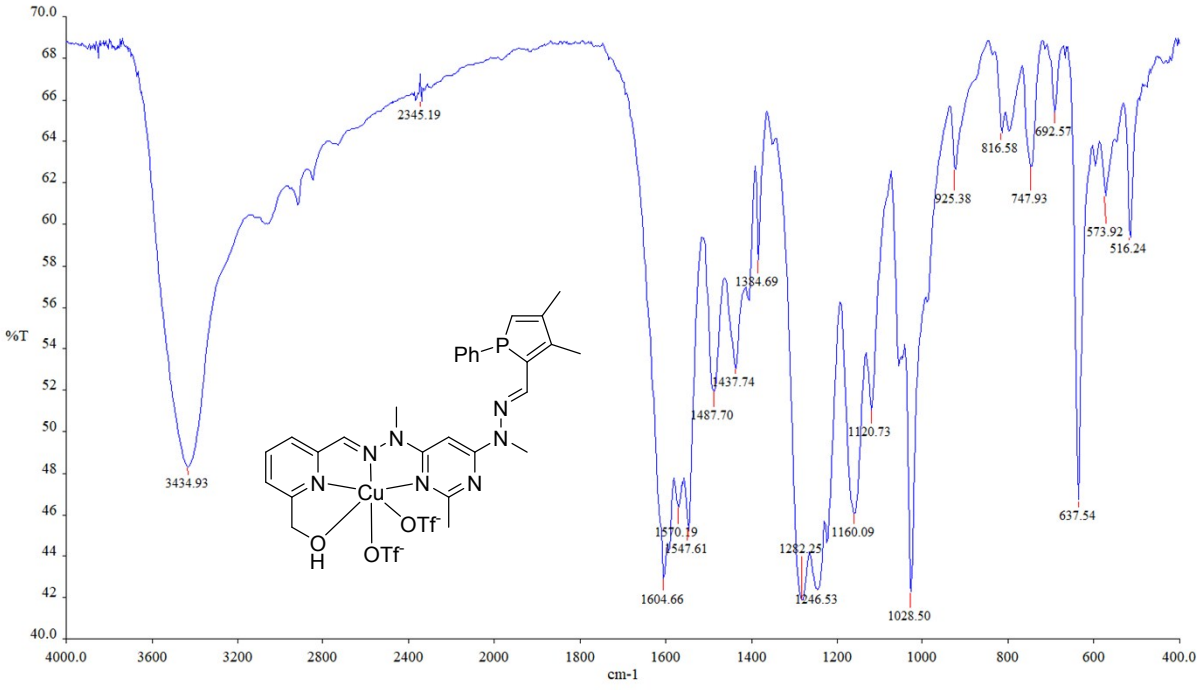

Figure 23. IR (KBr) spectrum of [Cu**L1**$(SO_3CF_3)_2$].

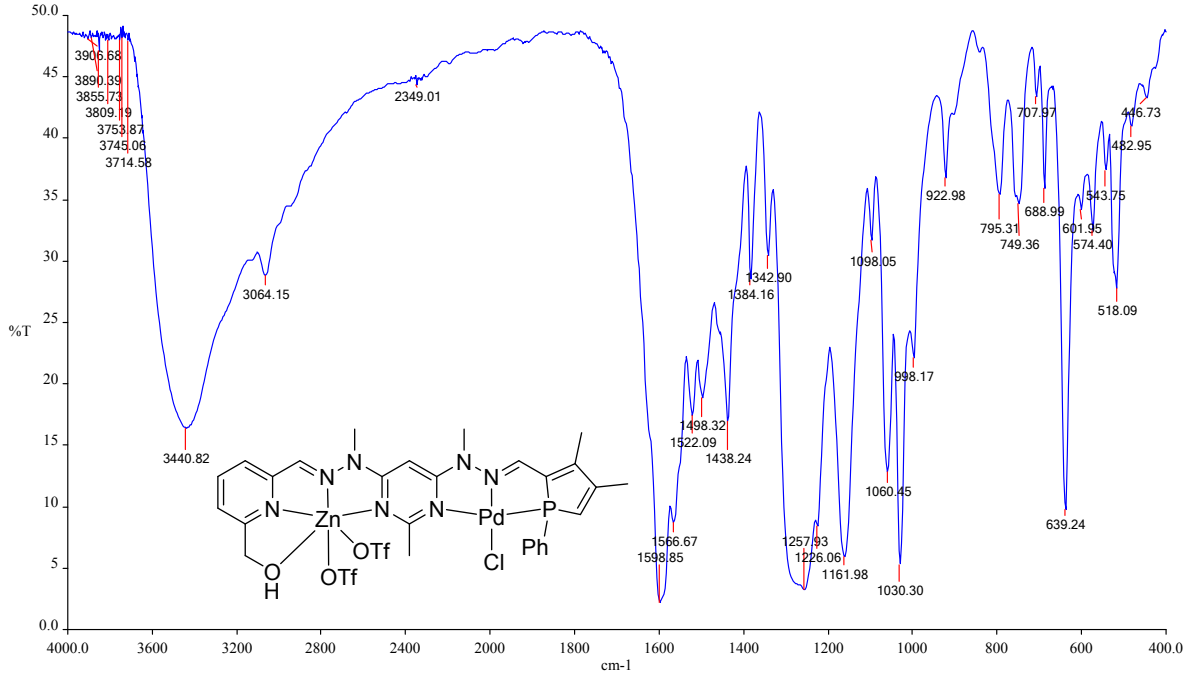

Figure S24. IR (KBr) spectrum of [ZnPd**L1**$Cl_2(SO_3CF_3)_2$].

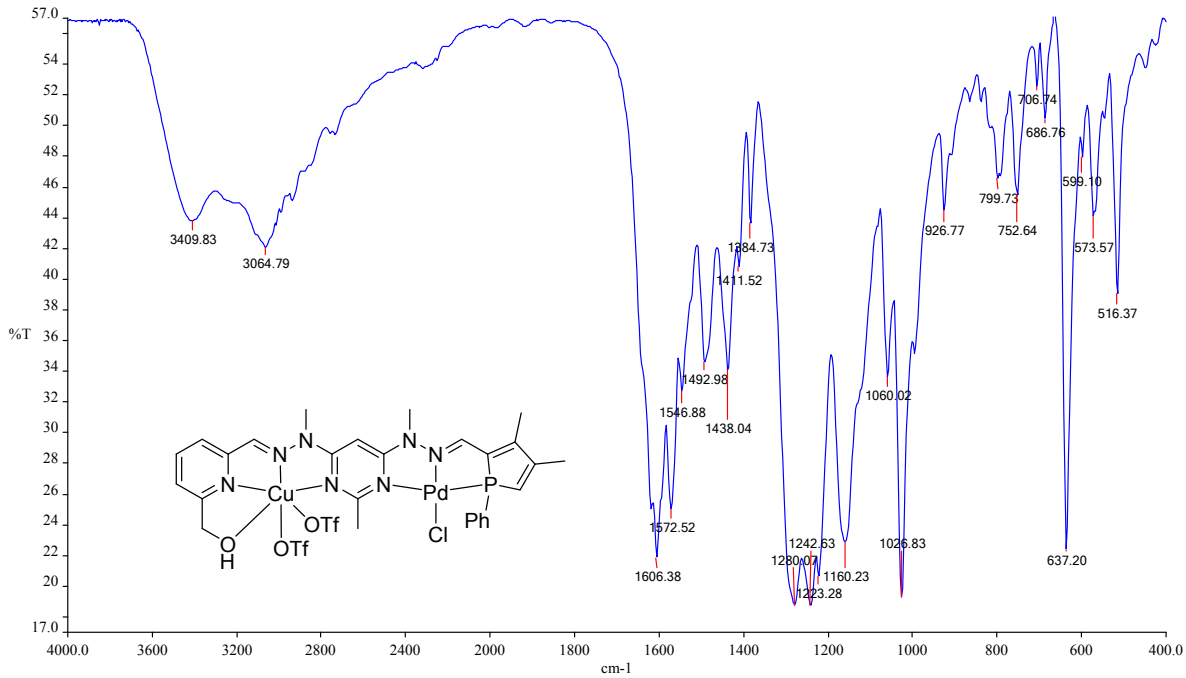

Figure S25. IR (KBr) spectrum of [CuPd**L1**$Cl_2(SO_3CF_3)_2$].

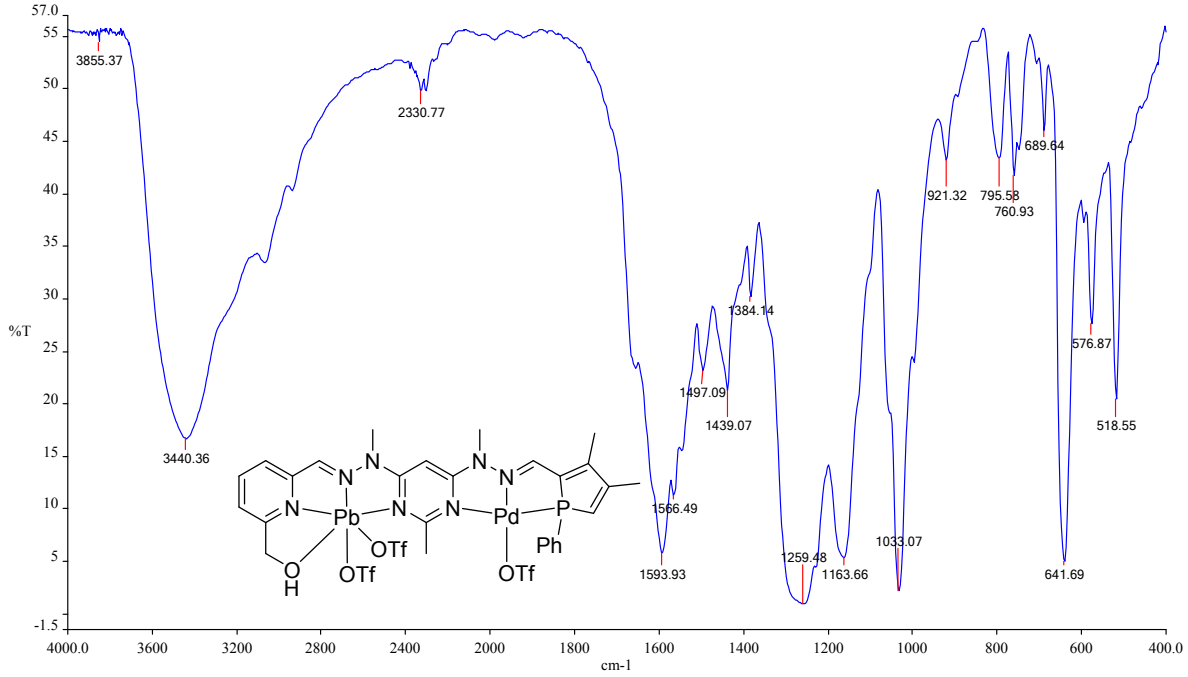

Figure S26. IR (KBr) spectrum of [PbPd**L1**$(SO_3CF_3)_4$].

5. ESMS data of L1 and its complexes

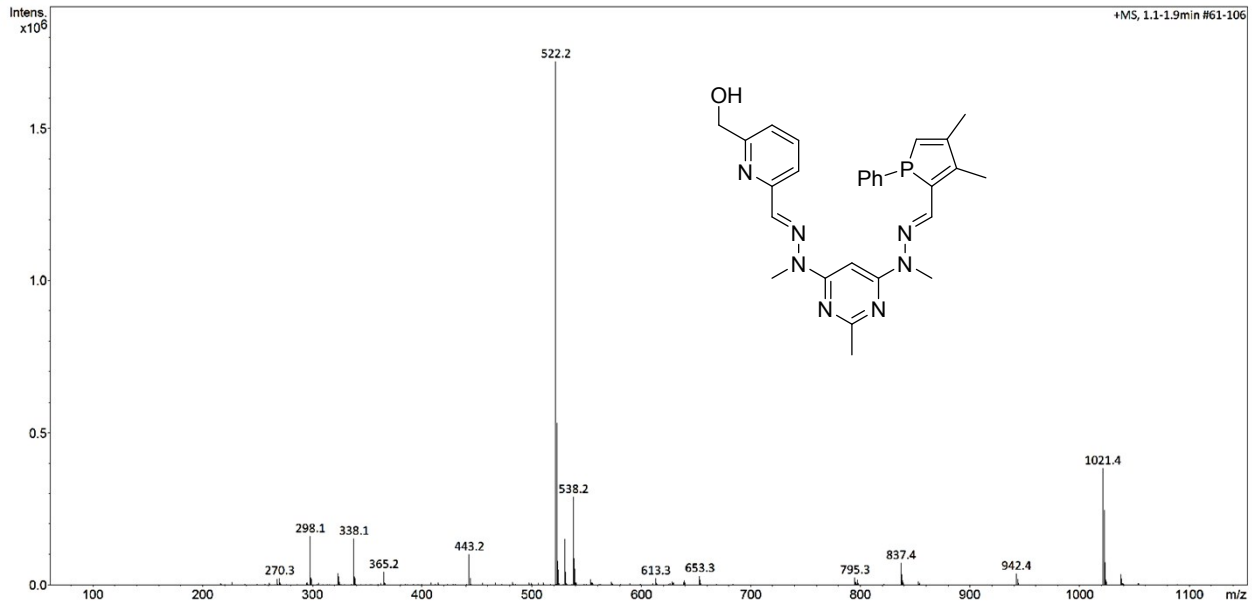

Figure S27. MS (ESI+) spectrum of **L1**.

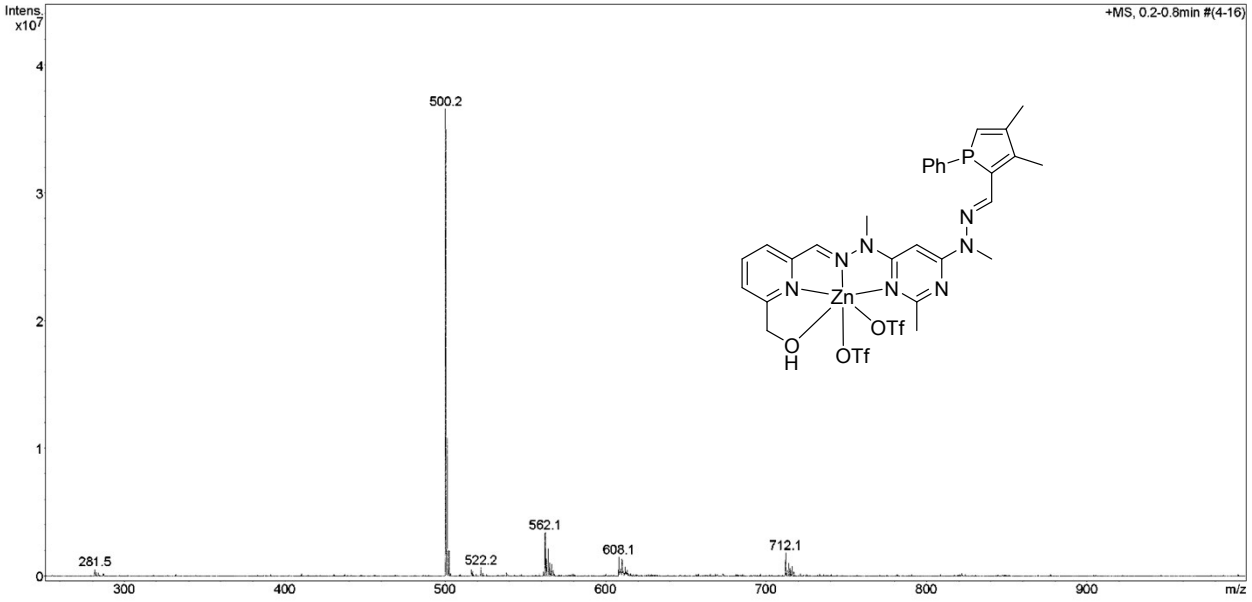

Figure S28. MS (ESI+) spectrum of [Zn**L1**$(SO_3CF_3)_2$].

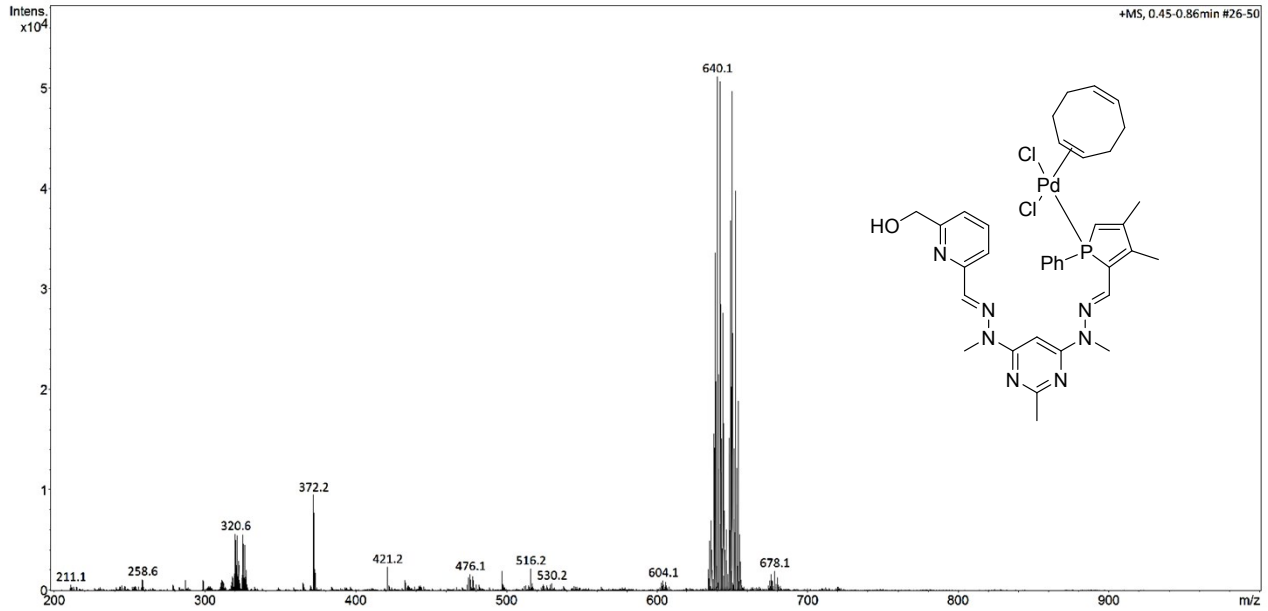

Figure S29. MS (ESI+) spectrum of [Pd**L1**Cl_2(COD)].

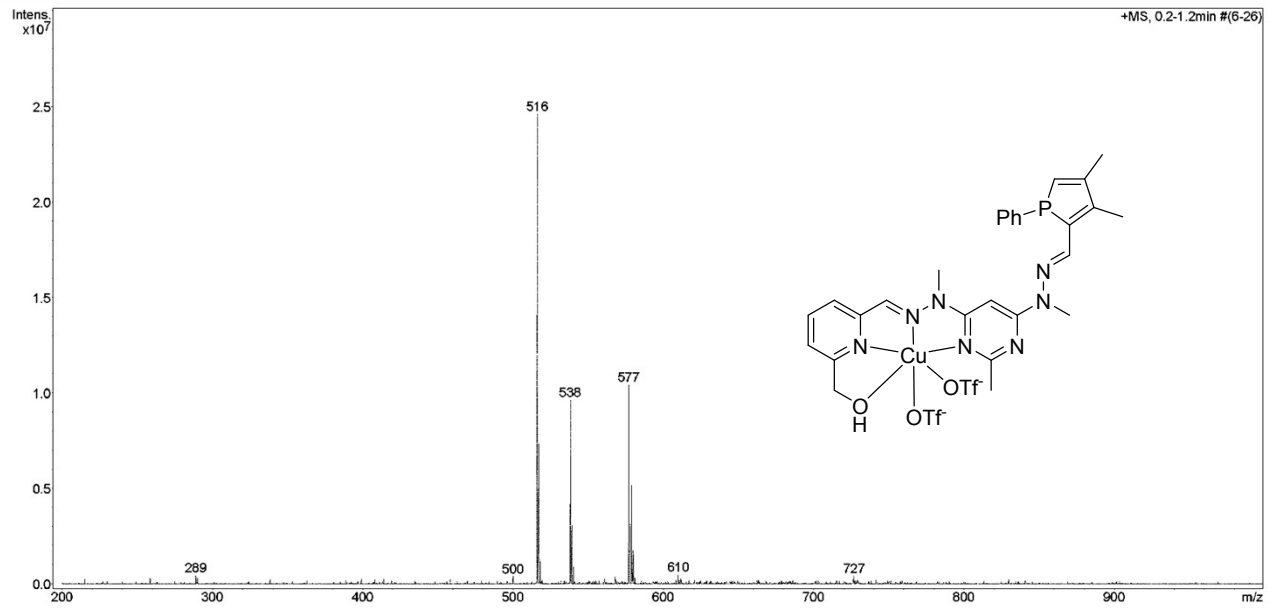

Figure S30. MS (ESI+) spectrum of [Cu**L1**$(SO_3CF_3)_2$].

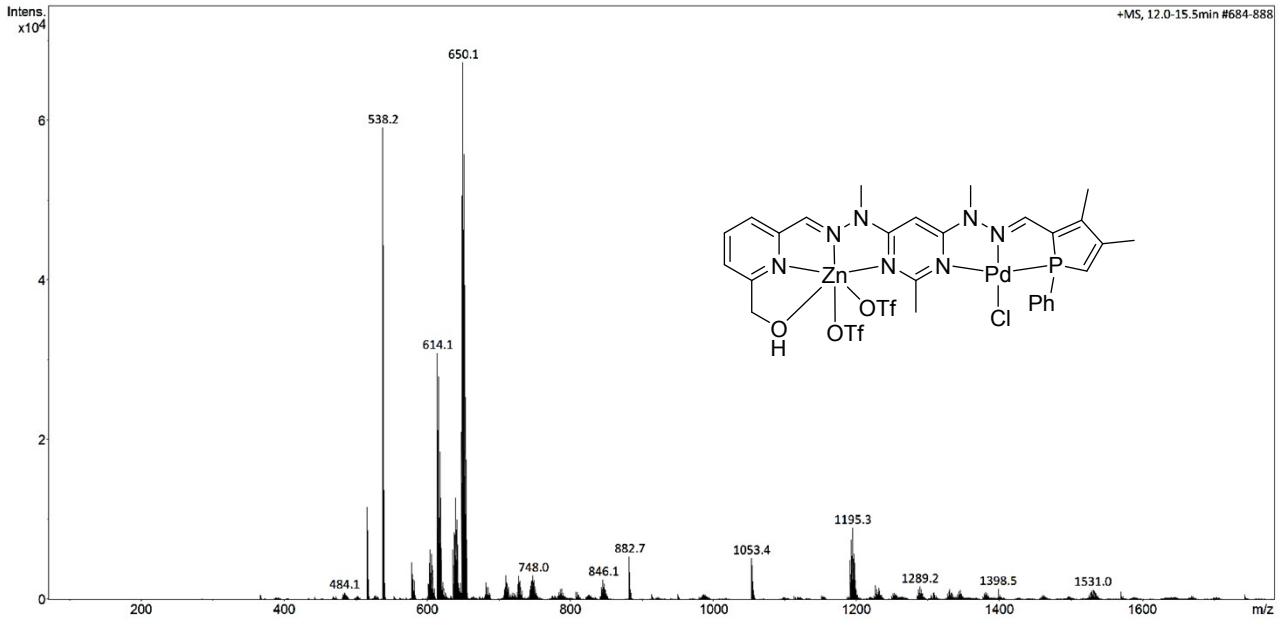

Figure S31. MS (ESI+) spectrum of [ZnPd**L1**$Cl_2(SO_3CF_3)_2$].

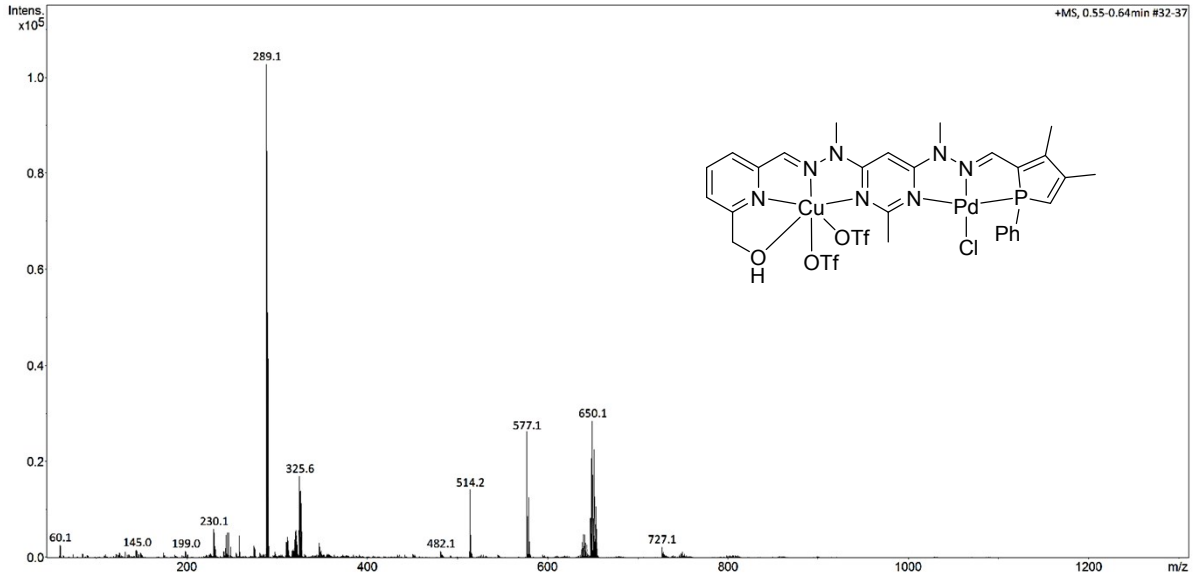

Figure S32. MS (ESI+) spectrum of [CuPd**L1**$Cl_2(SO_3CF_3)_2$].

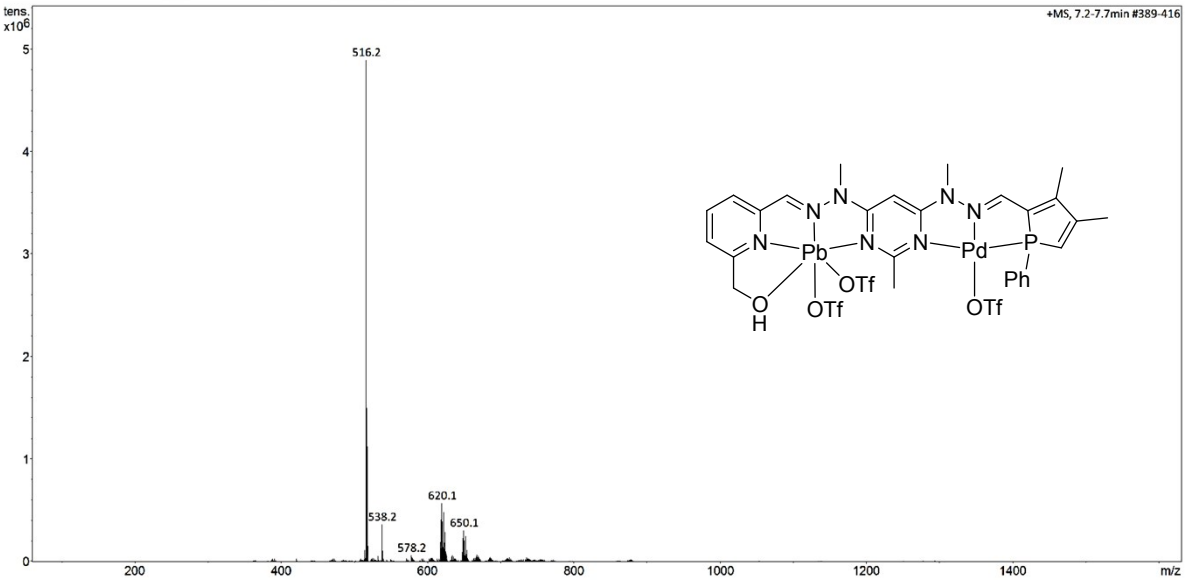

Figure S33. MS (ESI+) spectrum of [PbPd**L1**$(SO_3CF_3)_4$].

6. UV-vis data of the Cu^{II}-containing complexes of L1

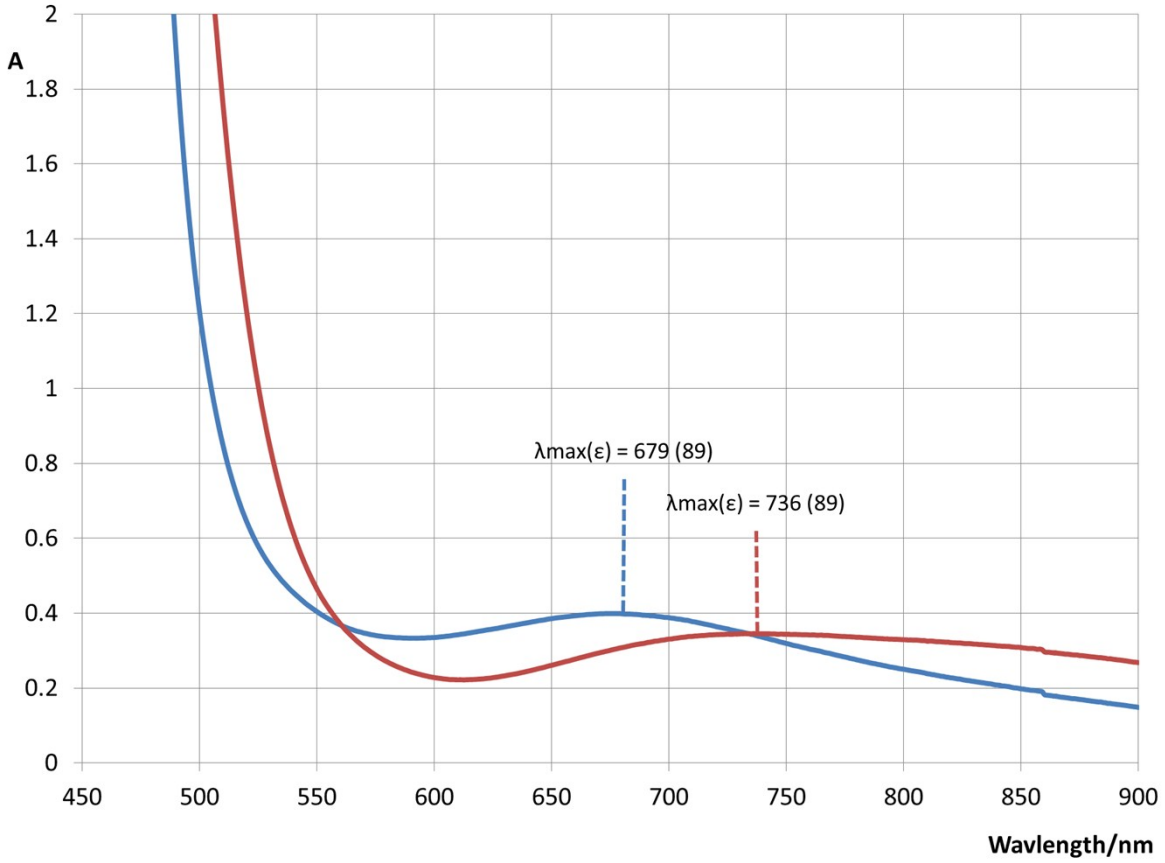

Figure S34. UV-vis spectra of [Cu**L1**$(SO_3CF_3)_2$] (blue) and [CuPd**L1**$Cl_2(SO_3CF_3)_2$] (red) in CH_3CN (concentrations of 4.45 and 3.85 $mmolL^{-1}$, respectively) with a path length of 1 cm.

7. GC-MS data from the Heck cCoupling and Miyaura borylation reactions

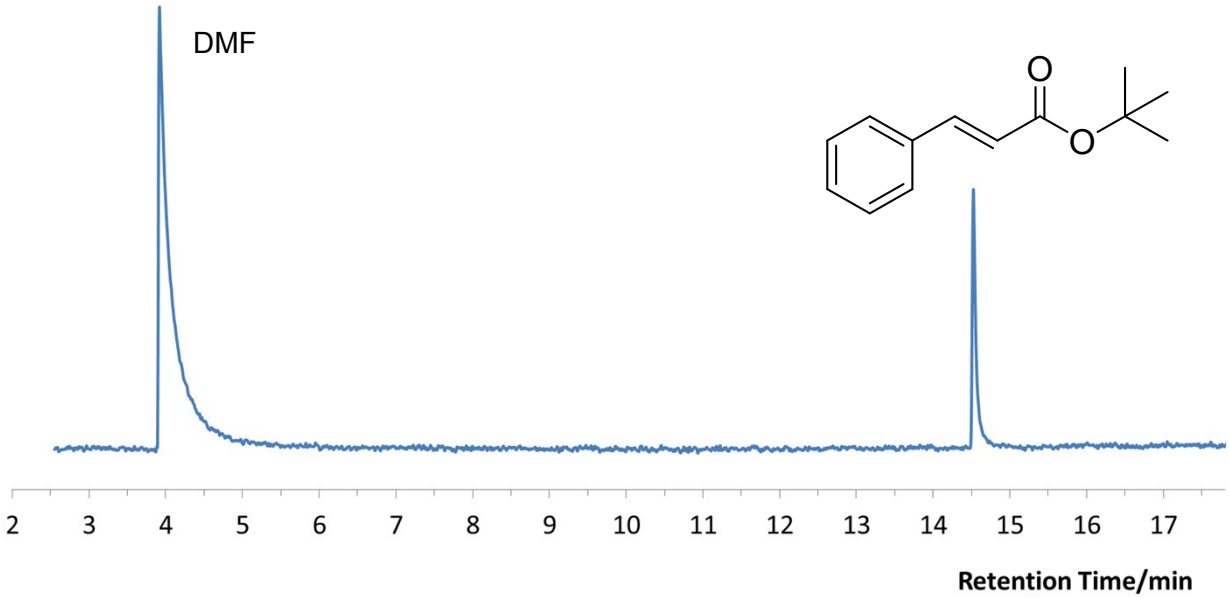

Figure S35. GC-MS plot of the products of the Heck reaction with iodobenzene catalysed by [ZnPd**L1**$Cl_2(SO_3CF_3)_2$]. Heating program: 50 °C (hold 2.5 min) / 6 °C·min^{-1} / 80 °C / 14 °C·min^{-1} / 180 °C (hold 2.0 min).

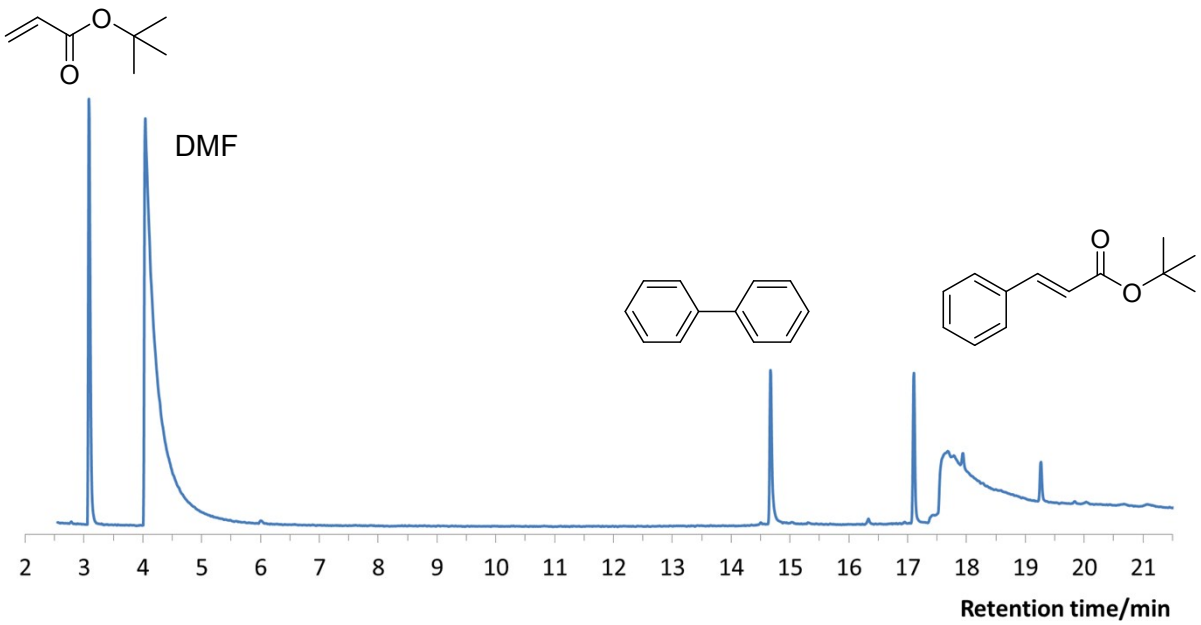

Figure S36. GC-MS plot of the products of the Heck reaction with bromobenzene catalysed by [ZnPd**L1**$Cl_2(SO_3CF_3)_2$]. Heating program: 50 °C (hold 2.5 min) / 6.15 °C min^{-1} / 80 °C (hold 0.30 min) / 10 °C min^{-1} / 150 °C (hold 0.30 min) / 6.00 °C min^{-1} / 180 °C (hold 3.0 min):

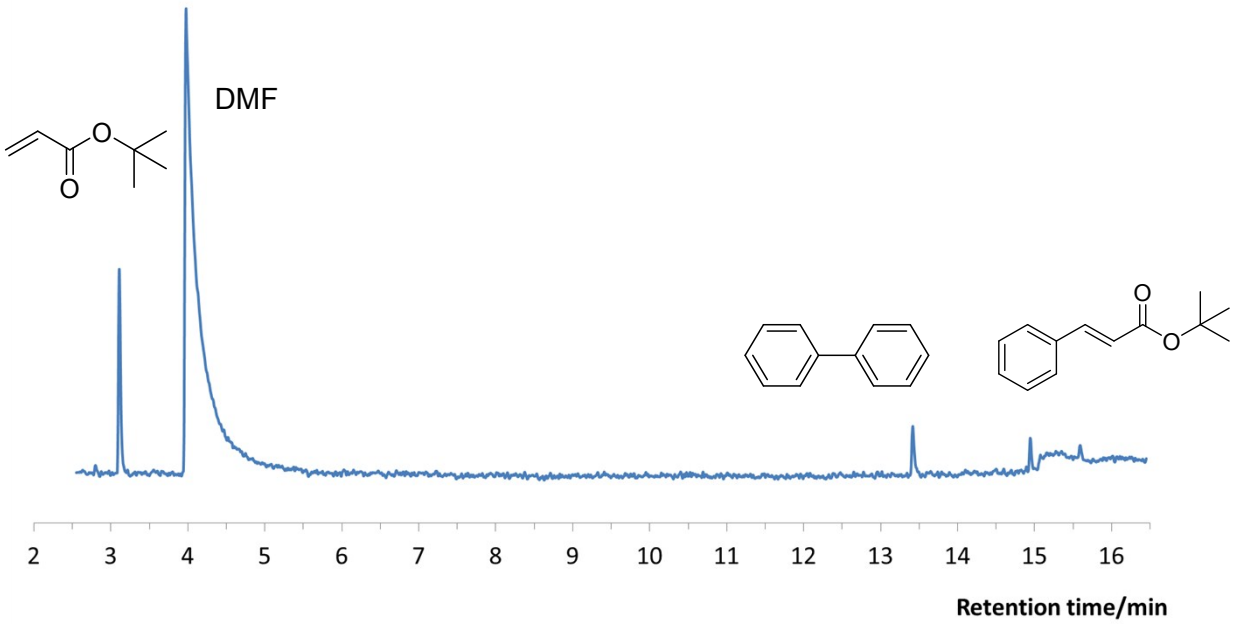

Figure S37. GC-MS plot of the products of the Heck reaction with bromobenzene catalysed by [CuPd**L1**$Cl_2(SO_3CF_3)_2$]. Heating program: 50 °C (hold 2.5 min) / 6 °C·min^{-1} / 80 °C / 14 °C·min^{-1} / 180 °C (hold 2.0 min).

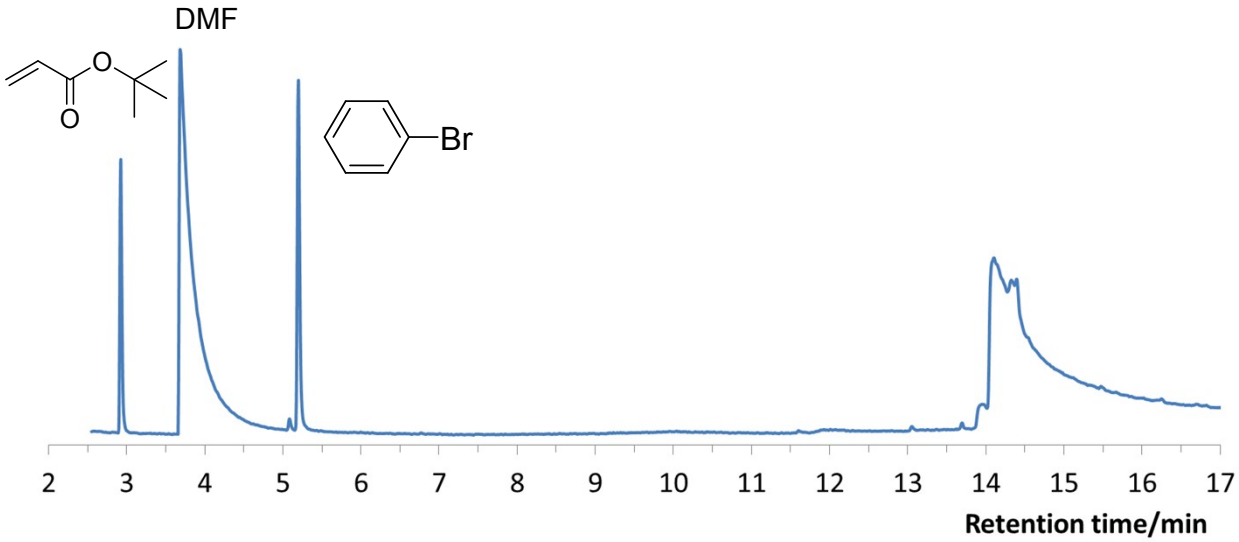

Figure S38. GC-MS plot of the products of the Heck reaction with bromobenzene catalysed by [PbPd**L1**$(SO_3CF_3)_4$]. Heating program: 50 °C (hold 2.5 min) / 6 °C·min^{-1} / 80 °C / 14 °C·min^{-1} / 180 °C (hold 2.0 min).

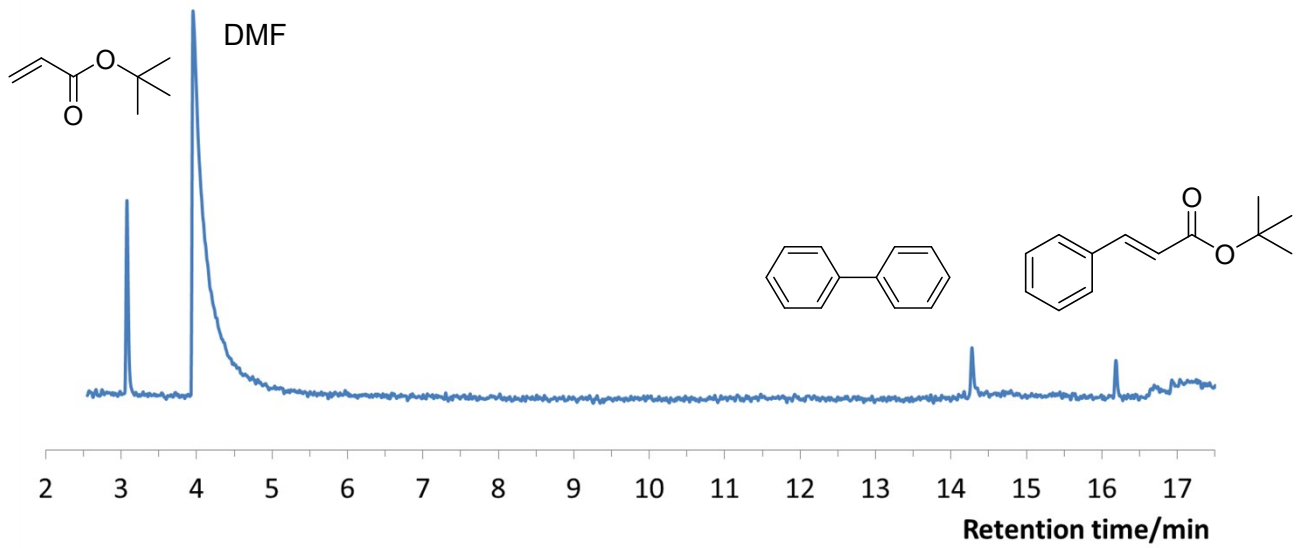

Figure S39. GC-MS plot of the products of the Heck reaction with bromobenzene catalysed by [Pd**L1**Cl_2(COD)]. Heating program: 50 °C (hold 2.5 min) / 6 °C·min^{-1} / 80 °C / 14 °C·min^{-1} / 180 °C (hold 2.0 min).

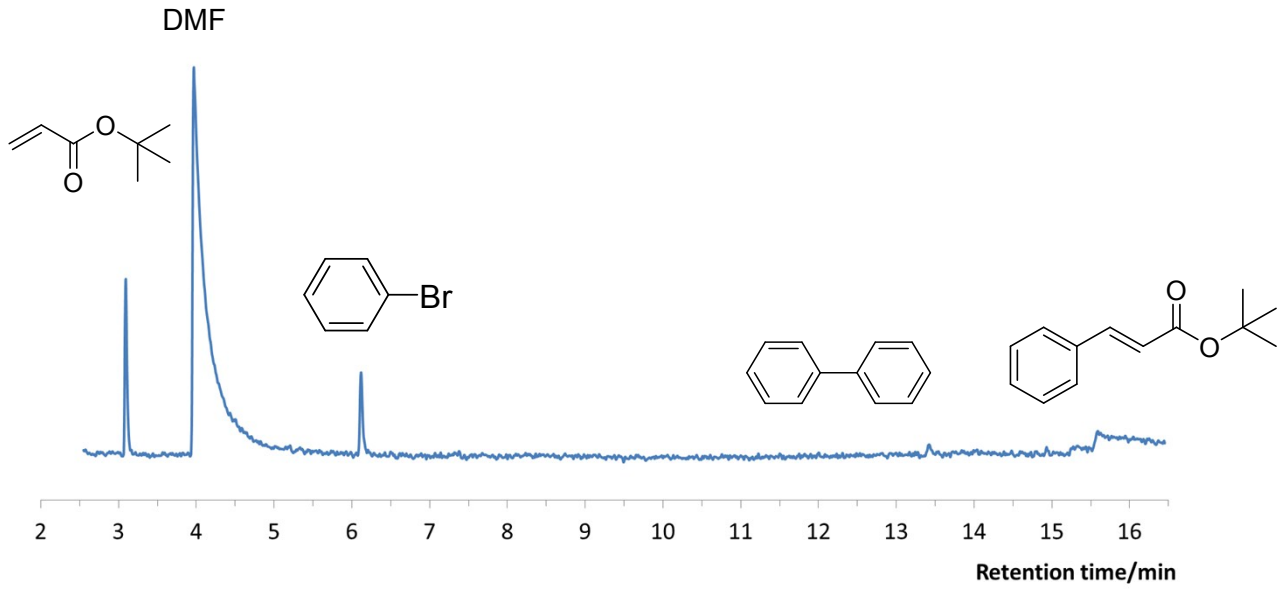

Figure S40. GC-MS plot of the products of the Heck reaction with bromobenzene catalysed by [$PdCl_2$(COD)]. Heating program: 50 °C (hold 2.5 min) / 6 °C·min^{-1} / 80 °C / 14 °C·min^{-1} / 180 °C (hold 2.0 min).

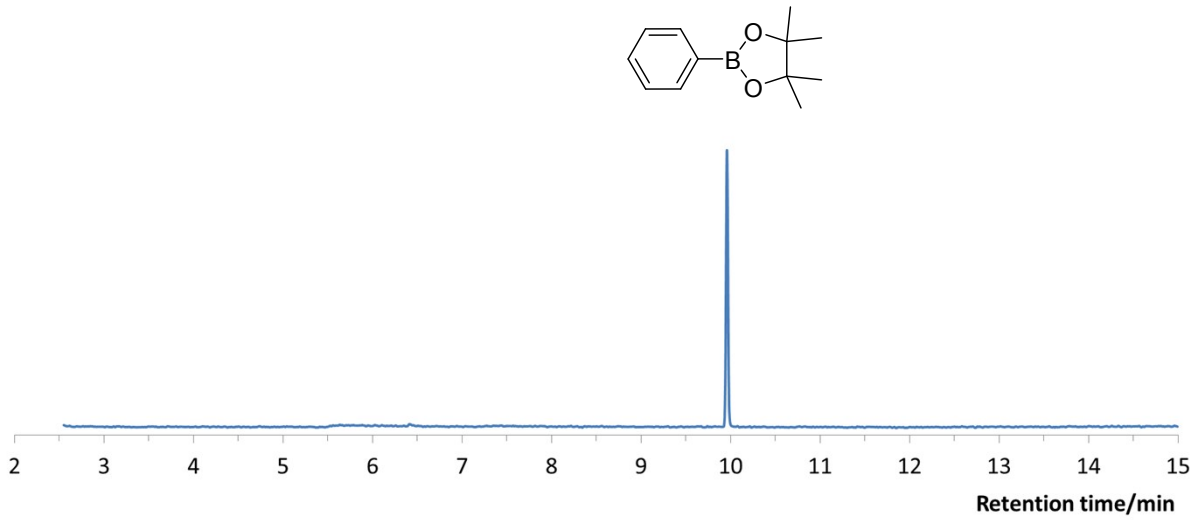

Figure S41. GC-MS plot of the products of the Miyaura borylation reaction with iodobenzene catalysed by [PdZn**L1**$Cl_2(SO_3CF_3)_2$]. Heating program: 50 °C (hold 2.0 min) / 13 °C·min^{-1} / 150 °C (hold 1.0 min) / 13 °C·min^{-1} / 180 °C (hold 2.0 min).

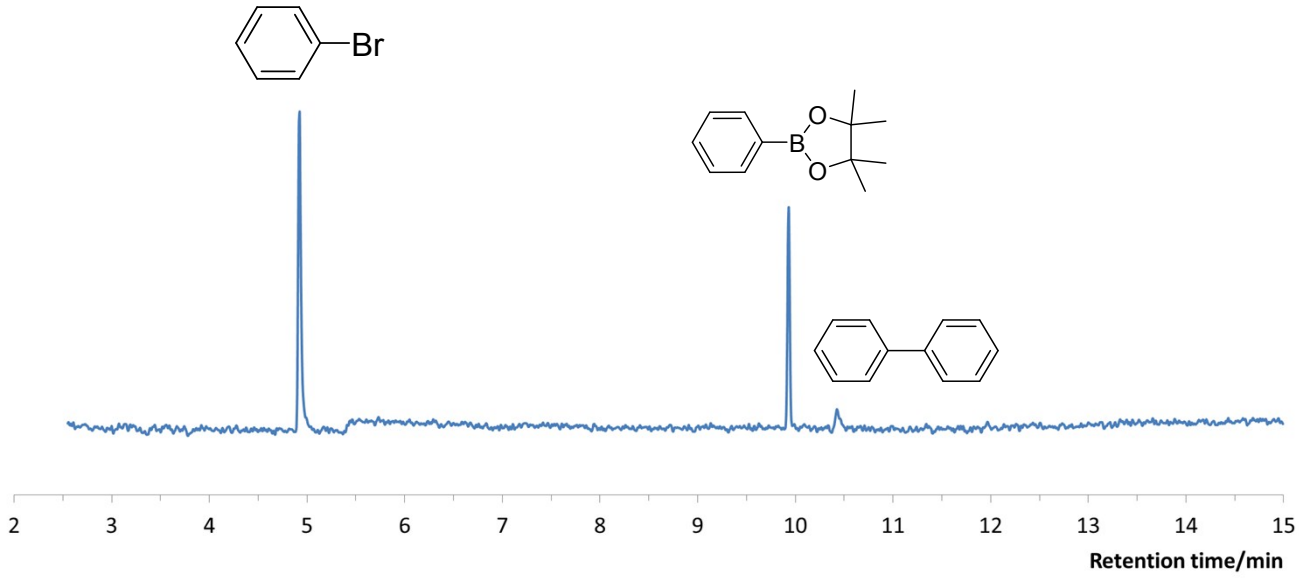

Figure S42. GC-MS plot of the products of the Miyaura borylation reaction with bromobenzene catalysed by [PdZn**L1**$Cl_2(SO_3CF_3)_2$]. Heating program: 50 °C (hold 2.0 min) / 13 °C·min^{-1} / 150 °C (hold 1.0 min) / 13 °C·min^{-1} / 180 °C (hold 2.0 min).